# MODELING OF QUANTUM PARALLEL RESONANT CONVERTERS - A NEW PARALLEL RESONANT CONVERTERS CONTROLLED BY INTEGRAL CYCLE MODE

Gyu B. Joung and Gyu H. Cho

Department of Electrical Engineering Korea Advanced
Institute of Science and Technology
P.O. Box 150 Chongryang Seoul 131-650, Korea

## ABSTRACT

Quantum parallel resonant converters(QPRC's), a dual converter of quantum series resonant converter(QSRC) and a subset of parallel resonant converters(PRC's) operating on zero voltage switching conditions, are modeled. It is shown that the QPRC can be operated as Cuk converter with an equivalent capacitor, buck or buck-boost converter with an additional equivalent capacitor. Modeling of these converters is verified through analysis and simulation results of the PRC. It is meant that the QPRC is modeled as Cuk, buck or buck-boost converter. Dc and ac characteristics of the quantum PRC's can be given by these models. Therefore, the QPRC can be designed similar to the QSRC to be controlled with closed loop feedback, having many advantages such as low device switching stress, reliable high frequency operation and low EMI, etc.

## I. INTRODUCTION

It is well known that resonant converters have many advantages over those of the conventional PWM converters[1-8]. However, conventional frequency[6] or phase[5] controlled resonant converters have some severe switching stresses and switching losses against varying frequency and phase difference.

Recently, quasi-resonant converter[3] and zero voltage switched converter[4] have been suggested and actively studied for optimized switching such as low switching stress and switching loss. However, modeling of such resonant converters is complex because of their non-linear characteristics against load and switching conditions, which makes it difficult to control the output voltage. Quantum resonant converters are also suggested for optimized switching[1,2] and quantum series resonant converter(QSRC) is modeled as general dc/dc converter with an equivalent inductance[1].

In this paper, quantum parallel resonant converter(QPRC) which has Cuk, buck or boost converter characteristics is suggested, analyzed and modeled. Output voltage of the QPRC can be controlled by discrete duty cycle similar to those of the case of QSRC. This model is verified by analytical and simulated comparisons between QPRC's and equivalent modeled PWM converters. Using the suggested model, it is shown that the output voltage of the QPRC's can be controlled by a proper feedback control scheme similar to the equivalent dc/dc converters. QPRC can be controlled to have nearly zero device voltage switching stress and switching loss, reliable high frequency operation and low EMI with variable output voltage by proper feedback algorithm, which are the distinctive features of the QPRC.

## II. SWITCH MODES OF PRC

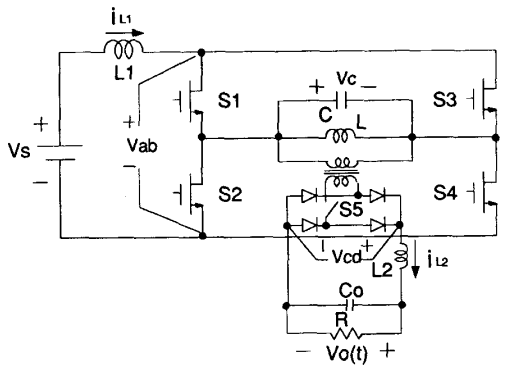


Fig. 1 Power circuit topology of PRC.

The power circuit topology of the PRC is suggested in Fig. 1. In this figure, additional switch S5 is added to the conventional PRC for the quantum Cuk PRC operation. When the PRC operates on optimal switching conditions, the switch pairs are turned on/off in synchronization with the voltage zero crossing points. Switch modes of the PRC have to be changed for every half resonant period for optimal switching condition[2]. The PRC with S5 has nine distinct modes as shown in Fig. 2. The description is as follows:

(A) Energizing mode : energizing modes are defined when S1,S4 and S2,S3 pairs are turned on/off alternately in synchronization with voltage zero crossing points of resonant capacitor voltage and S5 may be closed or open. When



CH2721-9/89/0000-0744 $1.00 © 1989 IEEE

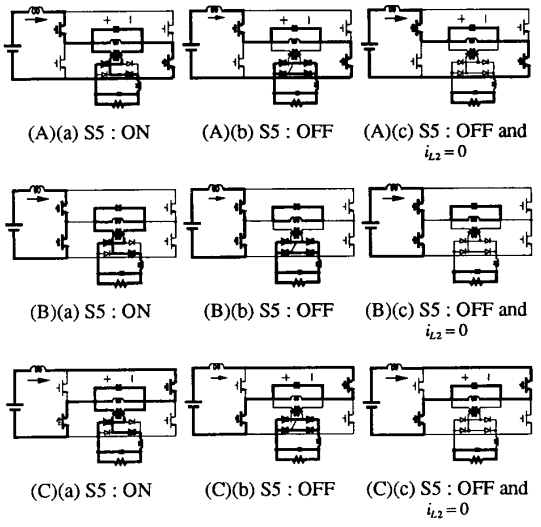


Fig. 2 Switch modes of PRC : (A) energizing mode. (B) de-energizing mode (C) regeneration mode.

S5 is closed, resonant circuit is energized by the input inductor current $i_{L1}$ and delivers it to the output through the inductor $L2$ as shown in Fig. 2(A)(a). If S5 is open state, the resonant circuit is energized by the input inductor current $i_{L1}$, however, the output current freewheels through the rectifier diodes as shown Fig. 2(A)(b). Therefore, this mode is named as energizing mode. If the output inductor current reaches zero, the switch mode may be changed depending on resonant capacitor voltage for resonant half period. If the capacitor voltage is lower than the output voltage $v_o$, $i_{L2}$ maintains zero as shown in Fig. 2(A)(c). If the capacitor voltage is higher than the output voltage, $i_{L2}$ starts to flow as shown in Fig. 2(A)(a) or (b) if S5 is closed.

(B) De-energizing mode : de-energizing modes are defined when S1,S3 and S2,S4 pairs are turned on/off alternately in synchronization with zero crossing points of resonant capacitor voltage. Also in this case S5 can be closed or open. During S5 is closed, the resonant circuit is de-energizied by the output inductor current $i_{L2}$ as shown in Fig. 2(B)(a). When S5 is open, the resonant current is circulated with constant energy as shown in Fig. 2(A)(b) and the output inductor current $i_{L2}$ freewheels through the rectifier diodes. If the output inductor current reaches zero, the switch mode can be changed depending on the resonant capacitor voltage. If the capacitor voltage is lower than the output voltage , $i_{L2}$ maintains zero as shown in Fig. 2(B)(c). If the capacitor voltage becomes higher than the output voltage, $i_{L2}$ starts increasing as shown in Fig. 2(B)(a) or (b) if S5 is closed.

(C) Regeneration mode : regeneration modes are defined when S2,S3 and S1,S4 pairs are turned on/off alternately in synchronization with zero crossing points of the resonant capacitor voltage. Also in this case S5 can be closed or open. During this mode, voltage and current of the resonant circuit are out of phase. When S5 is closed, the resonant circuit energy is transferred to the source and part of the energy is delivered to the load as shown in Fig. 2(C)(a). When S5 is open, the resonant circuit energy is transferred to the source and the output inductor current freewheels through the rectifier diodes as shown in Fig. 2(C)(b). If the output filter current reaches zero, the switch mode can be changed depending on the state of the resonant capacitor voltage for the resonant half period. If the capacitor voltage is lower than the output voltage , $i_{L2}$ maintains zero as shown in Fig. 2(C)(c). If the capacitor voltage is higher than the output voltage, $i_{L2}$ increases from zero as shown in Fig. 2(C)(a) or (b) if S5 is closed.

Table II. Transfer function of QPRC

| switch operation | | circuit variables | | | | |
|---|---|---|---|---|---|---|
| modes | States | $v_{ab}$ | $v_{cd}$ | $P_i$ | $P_o$ | $P_i - P_o$ |
| energizing mode | S5:ON, $i_{L2}>0$ | $\lvert v_c \rvert$ | $\lvert v_c \rvert$ | $\lvert v_c \rvert \cdot i_{L1}$ | $\lvert v_c \rvert \cdot i_{L2}$ | $\lvert v_c \rvert \cdot (i_{L1}-i_{L2})$ |
| | S5:OFF, $i_{L2}>0$ | | 0 | | 0 | $\lvert v_c \rvert \cdot i_{L1}$ |
| | $i_{L2}=0$ | | $\lvert v_o \rvert$ | | 0 | $\lvert v_c \rvert \cdot i_{L1}$ |
| de-energizing mode | S5:ON, $i_{L2}>0$ | 0 | $\lvert v_c \rvert$ | 0 | $\lvert v_c \rvert \cdot i_{L2}$ | $-\lvert v_c \rvert \cdot i_{L2}$ |
| | S5:OFF, $i_{L2}>0$ | | 0 | | 0 | 0 |
| | $i_{L2}=0$ | | $\lvert v_o \rvert$ | | 0 | 0 |
| regeneration mode | S5:ON, $i_{L2}>0$ | $-\lvert v_c \rvert$ | $\lvert v_c \rvert$ | $-\lvert v_c \rvert \cdot i_{L1}$ | $\lvert v_c \rvert \cdot i_{L2}$ | $-\lvert v_c \rvert \cdot (i_{L1}+i_{L2})$ |
| | S5:OFF, $i_{L2}>0$ | | 0 | | 0 | $-\lvert v_c \rvert \cdot i_{L1}$ |
| | $i_{L2}=0$ | | $\lvert v_o \rvert$ | | 0 | $-\lvert v_c \rvert \cdot i_{L1}$ |

* $P_i$ : input power of resonant circuit
* $P_o$ : output power of resonant circuit

The mode characteristics of the PRC are summarized in Table I. From this Table, the output voltage of the PRC can be controlled by moderate selection of the switch modes. Mode selection is allowed only at voltage zero crossing points, thus mode can be changed on every half resonant period as the QSRC[1,2]. The QPRC with S5 has six control modes. Thus, there exist many combinations to control and an optimal control pattern as a function of output voltage and load can be given. In the next sections, the switch modes are analyzed and PRC is modeled as conventional Cuk, buck or buck-boost converter with an equivalent filter capacitors.

## III. Analysis of the QPRC

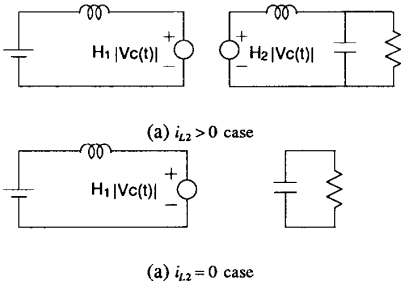


Fig.3 Equivalent circuit of switch modes for PRC.

Equivalent circuits of the PRC switch modes are shown in Fig. 3. These consist of two parts which are equivalent input and output circuits. The equivalent input circuits

include input voltage source $V_s$, input filter L1 and voltage $v_{ab}$ and the equivalent output circuits include voltage $v_{cd}$, filter L, C and loads. In these circuits, the voltage $v_{ab}$ and $v_{cd}$ are depending variables of the switch modes. Fig. 3(b) is the case when the output inductor current reaches zero. In these circuits, the voltage $v_{ab}$ is equal to $|v_c(t)|$ for the energizing mode, $-|v_c(t)|$ for the regeneration mode and zero for the de-energizing mode, respectively, because of their switching characteristics as shown in Table I. Therefore, the voltage $v_{ab}$ is rewritten by $H_1 \cdot |v_c(t)|$ and the voltage $v_{cd}$ by $H_2 \cdot |v_c(t)|$ as shown in Fig. 3. In this case, switching function $H_1$ is equal to unity for the energizing mode, zero for the de-energizing mode and -1 for the regeneration mode, respectively, and $H_2$ is equal to zero at S5 off and unity at S5 on.

The switch modes of the PRC can be analyzed by low ripple approximation method[7] because the inductances of L1 and L2 are usually sufficiently larger than the resonant inductance L. During the half resonant period T/2, the $|v_c(t)|$ is half sinusoidal. If we neglect the high frequency ripple components, the $|v_{co}(t)|$ can be given as follows:

$$v_{co}(t) = v_{co}(k) = |v_{cav}(k)| = \frac{2}{\pi}|v_{cp}(k)|$$

$$= \frac{2}{T}\int_{kT/2}^{kT/2+T/2} |v_c(t)|\,dt \quad kT/2 \le t < (k+1)T/2 \quad (1)$$

where $v_{cp}(k)$ and $v_{cav}(k)$ are peak and average values of the capacitor voltage during the k-th half resonant period, respectively.

A. Continuous current state of the filter inductor $L2$

The equivalent circuits correspond to Fig. 3(a). From this figure, we can neglect the high frequency ripple components of the $i_{L1}(t)$ if L1 >> L. During the k-th resonant period, the resonant voltage $v_c(t)$ becomes

$$|v_c(t)| = Z(i_L^*(k) + H_1 i_{L1}(k) - H_2 i_{L2}(k))\sin\{\omega_r(t - kT/2)\} \quad (2)$$

where $Z = \sqrt{L/C}$, $i_L^*(k)$ is the absolute value of the resonant current, $i_{L1}(k)$ and $i_{L2}(k)$ are the input or output filter current during of the k-th resonant period. Thus, absolute value of the average capacitor voltage $v_{co}(k)$ for the k-th resonant period becomes

$$v_{co}(k) = \frac{2Z}{\pi}\{i_L^*(k) + H_1 i_{L1}(k) - H_2 i_{L2}(k)\}. \quad (3)$$

From eq. (2), $i_L^*(k+1)$ becomes

$$i_L^*(k+1) = \frac{1}{L}\int_{kT/2}^{kT/2+T/2} Z\{i_L^*(k) + H_1 i_{L1}(k) - H_2 i_{L2}(k)\}\sin\{\omega_r(t - kT/2)\}dt$$

$$= i_L^*(k) + 2H_1 i_{L1}(k) - 2H_2 i_{L2}(k)\,. \quad (4)$$

From eq.(3) and (4),

$$v_{co}(k+1) = \frac{2Z}{\pi}\{i_L^*(k+1) + H_1 i_{L1}(k+1) - H_2 i_{L2}(k+1)\}$$

$$= v_{co}(k) + \frac{2Z}{\pi} H_1\{i_{L2}(k) + i_{L2}(k+1)\}$$

$$- H_2\{i_{L2}(k) + i_{L2}(k+1)\}. \quad (5)$$

If we let

$$\dot{v}_{co}(t) = \frac{v_{co}(k+1) - v_{co}(k)}{T/2} \quad (6)$$

$$i_{L1}(k) = i_{L1}(k+1) = i_{L1}(t) \quad (7)$$

$$i_{L2}(k) = i_{L2}(k+1) = i_{L2}(t) \quad (8)$$

then eq. (5) is arranged as follows:

$$\dot{v}_{co}(t) = \{(2/\pi)^2/C\}\{H_1 i_{L1}(t) - H_2 i_{L2}(t)\}. \quad (9)$$

By applying KVL to input side of Fig. 3(a), the state equation becomes

$$V_s = L1\frac{di_{L1}(t)}{dt} + |v_c(t)|H_1$$

$$= L1\frac{di_{L1}(t)}{dt} + v_{co}(t)H_1. \quad (10)$$

Because L1 >> L, the state equation is obtained by applying KCL to the output side and KVL of Fig. 3(a) as follow:

$$L2\frac{di_{L2}(t)}{dt} + v_o(t) = |v_c(t)|H_2 = v_{co}(t)H_2 \quad (11)$$

$$i_{L2} = C_o\frac{dv_o(t)}{dt} + \frac{v_o(t)}{R}. \quad (12)$$

From eq. (9), (10), (11) and (12), the state equations are obtained as follows:

$$\dot{X} = \begin{pmatrix} 0 & 0 & -H_1/L1 & 0 \\ 0 & 0 & H_2/L2 & -1/L2 \\ (2/\pi)^2 H_1/C & -(2/\pi)^2 H_2/C & 0 & 0 \\ 0 & 1/C_o & 0 & -1/RC_o \end{pmatrix} X + \begin{pmatrix} 1/L1 \\ 0 \\ 0 \\ 0 \end{pmatrix} V_s \quad (13)$$

where

$$X(t) = [\,i_{L1}(t) \quad i_{L2}(t) \quad v_{co}(t) \quad v_o(t)\,]^T \quad (14)$$

B. Discontinuous current state of $L2$

The equivalent circuits during this mode correspond to Fig. 3(b). In the input side of this figure, we can neglect the high frequency ripple components of the $i_{L1}$ and $i_{L2}$ if L1, L2 >> L. During the k-th resonant period, the output filter current $i_{L2}$ is zero and resonant voltage $v_c$ becomes

$$|v_c(t)| = Z(i_L^*(k) + H_1 i_{L1}(k))\sin\{\omega_r(t - kT/2)\} \quad (15)$$

The absolute value of the average capacitor voltage $v_{co}(k)$ for the k-th resonant period becomes

$$v_{co}(k)=\frac{2Z}{\pi}\{i_L^*(k)+H_1 i_{L1}(k)\}. \tag{16}$$

from eq. (15), $i_L^*(k+1)$ becomes

$$i_L^*(k+1)=\frac{1}{L}\int_{kT/2}^{kT/2+T/2} Z\{i_L^*(k)+H_1 i_{L1}(k)\}\sin\{\omega_r(t-kT/2)\}dt - i_L^*(k)$$

$$=i_L^*(k)+2H_1 i_{L1}(k). \tag{17}$$

From eq. (15) and (17), we obtain

$$v_{co}(k+1)=v_{co}(k)+\frac{2Z}{\pi}H_1\{i_{L1}(k)+i_{L1}(k+1)\}. \tag{18}$$

Eq. (6), (7) and (18) can be rearranged as

$$\dot{v}_{co}(t)=\{(2/\pi)^2/C\}H_1 i_{L1}(t). \tag{19}$$

The state equations at the output side of Fig. 3(b) are given as

$$\dot{i}_{L2}(t)=0 \tag{20}$$

$$0=C_o\frac{dv_o(t)}{dt}+\frac{v_o(t)}{R}. \tag{21}$$

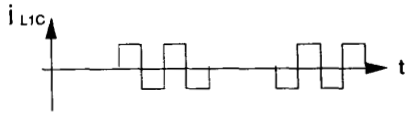


(a) resonant capacitor input current due to $i_{L1}$

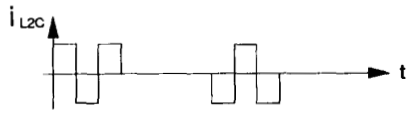


(b) resonant capacitor input current due to $i_{L2}$


(c) resonant capacitor voltage

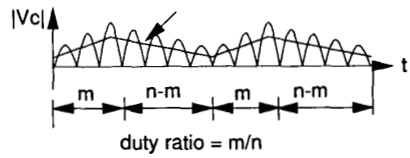


(c) rectified voltage of resonant capacitor

Fig. 4 Waveforms of Quantum Cuk PRC.

From eq. (10), (19),(20) and (21), we obtain the state equations as follows:

$$\dot{X}=\begin{pmatrix} 0 & 0 & -H_1/L1 & 0 \\ 0 & 0 & 0 & 0 \\ (2/\pi)^2H_1/C & 0 & 0 & 0 \\ 0 & 0 & 0 & -1/RC_o \end{pmatrix}X+\begin{pmatrix} 1/L1 \\ 0 \\ 0 \\ 0 \end{pmatrix}V_s \tag{22}$$

QPRC can be operated similar to the conventional Cuk characteristics and conventional buck/boost characteristics with an additional filter. These are discussed in next section.

## IV. QUANTUM CUK PRC

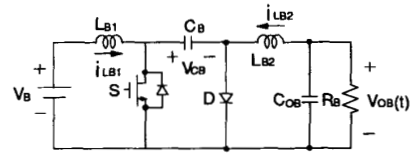


(a) conventional Cuk converter


(b) energy transfer capacitor current $i_{CB}$

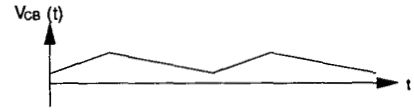


(c) energy transfer capacitor voltage $v_{CB}$

Fig. 5 Conventional Cuk converter and Waveforms of this.

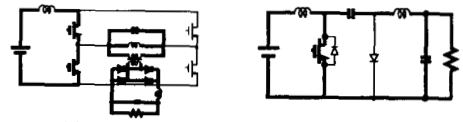

(a) switch mode comparison in active state

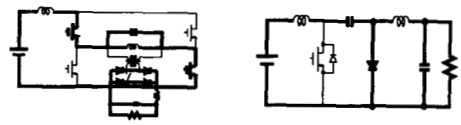

(b) switch mode comparison in passive state

Fig. 6 Switching state comparisons of the quantum Cuk PRC with conventional Cuk converter.

Switching patterns and equivalent capacitor voltage $|v_c(t)|$ of the quantum Cuk PRC are similar to the switching pattern and capacitor voltage $v_{CB}$ of the conventional Cuk converter as shown in Fig. 4 and 5. Fig. 6 shows switching state comparisons of the QPRC with conventional Cuk converter. As shown in Fig. 6, the output voltage of the quantum Cuk PRC can be controlled by selection of two switching states. Equivalent state of Cuk PRC when S5 is on correspond to Fig. 3(a) with $H_1=0$ and $H_2=1$ while that of S5 off correspond to $H_1=1$ and $H_2=0$. Since the filter inductors L1 and L2 are much larger than the resonant inductor L, the general state equations eq. (13) can be approximated as follows :

$$\dot{X}=\begin{pmatrix} 0 & 0 & -H/L1 & 0 \\ 0 & 0 & \overline{H}/L2 & -1/L2 \\ (2/\pi)^2 H/C & -(2/\pi)^2\overline{H}/C & 0 & 0 \\ 0 & 1/C_o & 0 & -1/RC_o \end{pmatrix} X + \begin{pmatrix} 1/L1 \\ 0 \\ 0 \\ 0 \end{pmatrix} V_s \quad (23)$$

where the new switching function H is defined as follows :

(1) active mode ( $H_1=0$ and $H_2=1$ ) : $H=0$ and $\overline{H}=1$ ,
(2) passive mode ( $H_1=1$ and $H_2=0$ ) : $H=1$ and $\overline{H}=0$ .

The equations shown for the quantum Cuk PRC are similar to those of the conventional Cuk converter. The equivalent Cuk PRC operates as a conventional Cuk dc/dc converter with an equivalent inductance $L_B$ having the duty ratio quantized by the resonant half period for PWM operation as shown in Fig. 4. The equivalent circuit parameters of the quantum Cuk PRC are as follows:

$$C_B=\left(\frac{\pi}{2}\right)^2 C \quad (24-a)$$

$$L_{B1}=L1 \quad (24-b)$$

$$L_{B2}=L_2 \quad (24-c)$$

$$C_{CO}=C_O \quad (24-d)$$

$$R_B=R \quad (24-e)$$

## V. OTHER QUANTUM PARALLEL RESONANT CONVERTERS

A. Quantum buck PRC with an additional filter.

Quantum PRC operation with buck characteristics is proposed as shown in Fig. 7. In this case, S1, S4 and S2, S3 pairs are always turned on/off alternately and the output voltage is controlled by the additional switch S5. Therefore $H_1$ is always unity and $H_2$ is zero at S5 off state and $H_2$ is unity at S5 on. All of the switches operate in synchronization with the voltage zero crossing points. High frequency ripple components of the output side rectified voltage can also be neglected because of the larger filter inductors.

By applying similar method as the quantum Cuk PRC, we know that this converter operates as buck converter with an additional filter as shown in Fig. 7. The equivalent circuit parameters of the quantum buck PRC are as follows:

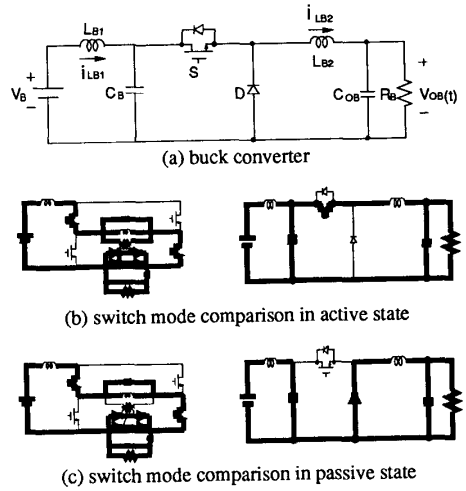


Fig. 7 Switching state comparisons of the quantum buck PRC with conventional buck converter with an input filter.

$$C_B=\left(\frac{\pi}{2}\right)^2 C \quad (25-a)$$

$$L_{B1}=L1 \quad (25-b)$$

$$L_{B2}=L_2 \quad (25-c)$$

$$C_{CO}=C_O \quad (25-d)$$

$$R_B=R \quad (25-e)$$

As mentioned above, the quantum PRC can be modeled as conventional buck converter with an equivalent capacitor $C_B$

B. Quantum Boost PRC with an additional filter.

The QPRC operation with boost characteristics is proposed as shown in Fig. 8. The modeling procedure is similar to those of shown above. In the quantum boost PRC operation, $H_2$ is always unity and $H_1$ is unity or zero depending on the S1 - S4 switching conditions. The equivalent circuit parameters are as follows:

$$C_B=\left(\frac{\pi}{2}\right)^2 C \quad (26-a)$$

$$L_{B1}=L1 \quad (26-b)$$

$$L_{B2}=L_2 \quad (26-c)$$

$$C_{CO}=C_O \quad (26-d)$$

$$R_B = R \qquad (26-e)$$

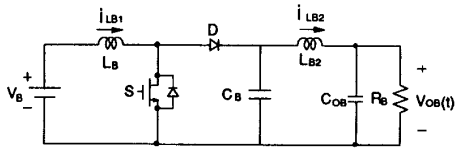


(a) boost converter

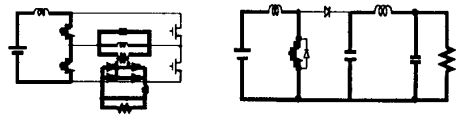

(b) switch mode comparison in active state

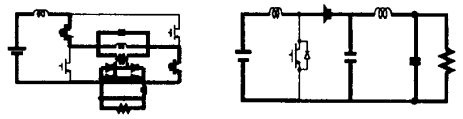

(c) switch mode comparison in passive state

Fig. 8 Switching state comparisons of the quantum boost PRC with conventional boost converter with an output filter.

From eq. (26) and Fig. 8, we know that the quantum boost PRC with an additional equivalent output filter capacitor $C_B$

C. QPRC with general switching pattern

There are other varieties to control the output voltage of the QPRC by proper selection of the switching functions ( $H_1$ and $H_2$ ). New operation of the QPRC is also possible using the equivalent circuit and the state variables given in Fig. 3 and eq. (13).

Table I. Mode Characteristics of PRC

| QPRC s | Transfer function | |
|---|---|---|
| | $G_v(S)$ | dc transfer function $G_v$ |
| quantum Cuk PRC | $G_v(S)=\frac{\alpha(1-D_c)D_c}{S^4+\beta_1S^3+\beta_2S^2+\beta_3S+\alpha(1-D_c)^2}$ | $G_v=\frac{D_c}{(1-D_c)}$ |
| quantum buck PRC | $G_v(S)=\frac{\alpha D_{BU}}{S^4+\beta_1S^3+\beta_4S^2+\beta_5S+\alpha}$ | $G_v=D_{BU}$ |
| quantum boost PRC | $G_v(S)=\frac{\alpha D_{BO}}{S^4+\beta_1S^3+\beta_6S^2+\beta_7S+\alpha D_{BO}^2}$ | $G_v=\frac{1}{D_{BO}}$ |

$\alpha=\frac{(2/\pi)^2}{L1L2C_o}$, $\beta_1=\frac{1}{RC_o}$, $\beta_2=\frac{1}{L2C_o}+\frac{(2/\pi)^2D_c^2}{L2C}$,

$\beta_3=-\frac{(2/\pi)^2\{(1-D_c)^2-D_c^2\}}{L2CC_oR}$, $\beta_4=\frac{1}{L2C_o}+\frac{(2/\pi)^2D_{BU}^2}{L2C}$,

$\beta_5=-\frac{(2/\pi)^2(1-D_{BU}^2)}{L2CC_oR}$, $\beta_6=\frac{1}{L2C_o}+\frac{(2/\pi)^2}{L2C}$,

$\beta_7=-(2/\pi)^2\frac{(D_{BO}^2-1)}{L2CC_oR}$.

* $D_c=m/n$, $D_{BU}=m/n$, $D_{BO}=m/n$.

where $m(T/2)$ is active period and $n(T/2)$ is total period of active and passive modes.

## VI. TRANSFER FUNCTION CHARACTERISTICS

From eq. (13), state equations of the QPRC are rearranged as follows:

$$\dot{X}(t)=A(H_1,H_2)X(t)+BV_s \qquad (27)$$

where

$$A=\begin{pmatrix}0 & 0 & -H_1/L1 & 0\\ 0 & 0 & H_2/L2 & -1/L2\\ (2/\pi)^2H_1/C & -(2/\pi)^2H_2/C & 0 & 0\\ 0 & 1/C_o & 0 & -1/RC_o\end{pmatrix} \quad B=\begin{pmatrix}1/L1\\0\\0\\0\end{pmatrix} \qquad (28)$$

By applying state space averaging methods[9], $A(H_1,H_2)$ is changed by $\overline{A}(\overline{H}_1,\overline{H}_2)$ as follows:

$$\overline{A}=\begin{pmatrix}0 & 0 & -\overline{H}_1/L1 & 0\\ 0 & 0 & \overline{H}_2/L2 & -1/L2\\ (2/\pi)^2\overline{H}_1/C & -(2/\pi)^2\overline{H}_2/C & 0 & 0\\ 0 & 1/C_o & 0 & -1/RC_o\end{pmatrix} \quad \overline{B}=\begin{pmatrix}1/L1\\0\\0\\0\end{pmatrix} \qquad (29)$$

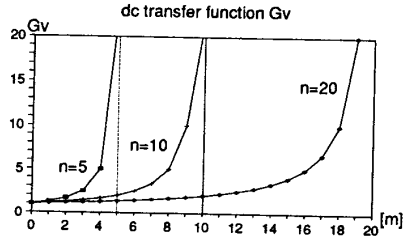


(a) quantum Cuk PRC

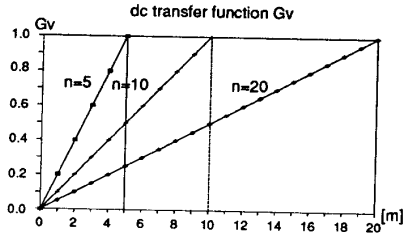


(b) quantum buck PRC

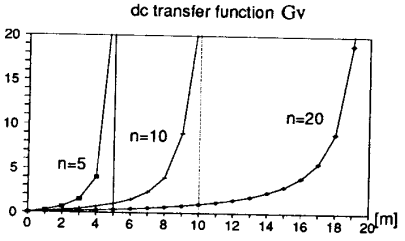


(c) quantum boost PRC

Fig. 9 Dc transfer function Gv of QPRC's.

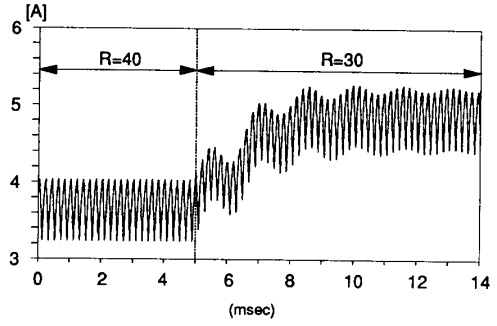


(a) inductor current $i_{L1}$

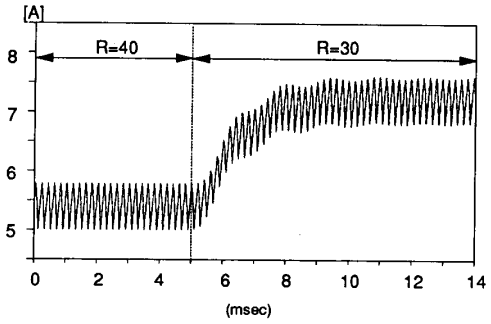


(b) inductor current $i_{L2}$

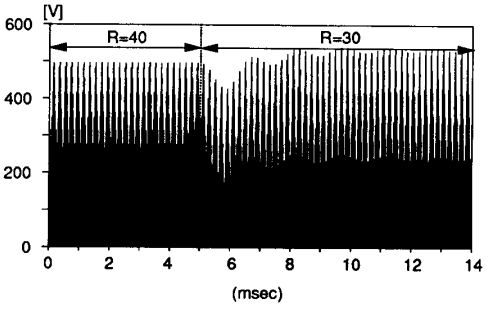


(c) absolute value of capacitor voltage $|v_C|$

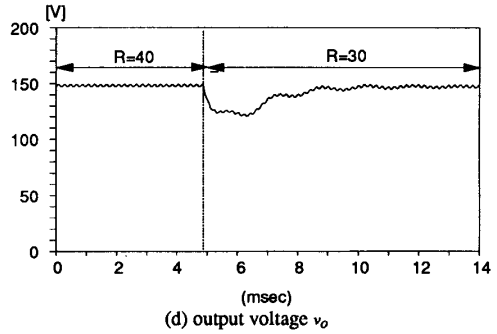


(d) output voltage $v_o$

(A) quantum Cuk PRC

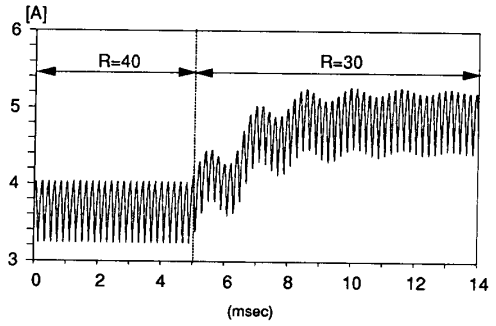


(a) inductor current $i_{LB1}$

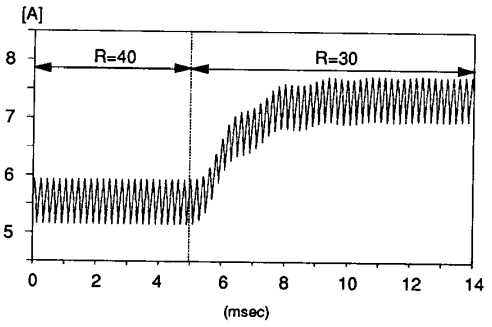


(b) inductor current $i_{LB2}$

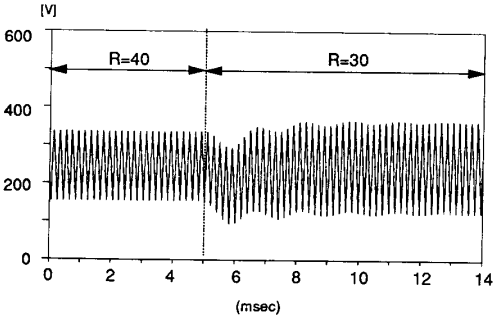


(c) capacitor voltage $v_{CB}$

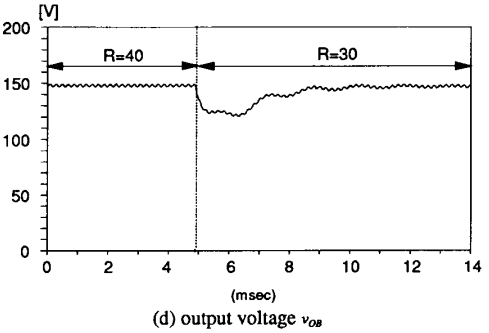


(d) output voltage $v_{OB}$

(B) modeled Cuk converter

Fig. 10 Simulation results of dynamic response : comparisons of quantum Cuk PRC with the modeled Cuk converter for absolute changing of load resistance from 40Ω to 30Ω, respectively.

where

$\overline{H}_1$ is average value of the $H_1$ and $\overline{H}_2$ is average value of the $H_2$.

From eq. (27), (28), and (29), the transfer function $G_v(S)$ of the output voltage to input voltage is

$$G_v(S) = \frac{(\frac{2}{\pi})^2 H_1 H_2}{L1L2CC_o} \Big/ S^4 + \frac{S^3}{RC_o} + \left\{\frac{1}{L2C_o} + \frac{(\frac{2}{\pi})^2 H_2^2}{L2C}\right\} S^2 - \left\{\frac{(\frac{2}{\pi})^2 (H_1^2 - H_2^2)}{L2CC_oR}\right\} S + \frac{(\frac{2}{\pi})^2 H_1}{L1L2CC_o} \quad (30)$$

From eq. (30), the transfer function $G_v(S)$ and dc transfer function Gv(S=0) of the quantum Cuk, buck and boost PRC can be obtained as Table II.

The dc transfer functions Gv are obtained as shown in Fig. 9. In these figures, the dc transfer functions correspond to those of equivalent Cuk, buck and boost converter except quantized levels caused by the quantized duty(m/n). If lower quantization level of the output voltage is desired, the number of n should be increased, however, the resonant current ripple generally increases for increasing n. Therefore, the optimal control pattern[8] for these converter needs some compromise between minimum ripple and minimum output voltage step.

## VII. SIMULATION RESULTS

For the dynamic comparison of the simulation result of quantum Cuk PRC and conventional Cuk converter with equivalent modeled parameters of QPRC, the quantum PRC are designed with $Z(=\sqrt{L/C}) = \sqrt{40}\Omega$ at 250KHz resonant frequency controlled with 50KHz modulation frequency. Thus, the number n representing the total modulation period as an integer multiple of half resonant period is ten. For comparison of simulation results, the conventional Cuk converter is equivalently operated at 50KHz. The actual parameter values of the quantum Cuk and the corresponding equivalent values to the conventional Cuk converter are as follows:

$V_S = 100$ $\quad V_B = 100$

$C = 0.1\mu F$ $\quad C_{OB} = (\pi/2)^2 C = 0.247\mu F$

$L = 4\mu H$

$L_{B1} = L_{B2} = 1.5mH$ $\quad L_{B1} = L_{B2} = 1.5mH$ : internal resistor ( $0.2\Omega$ )

$C_O = 1\mu F$ $\quad C_{OB} = 1\mu F$

Fig. 10 shows the dynamic comparisons of the simulation results for the quantum Cuk PRC and conventional Cuk converter where the parameters of the quantum Cuk PRC and the conventional Cuk converter are set to be equivalently equal. In this case simulated duty ratio of the quantum Cuk PRC is 6/10 and that of the modeled Cuk converter is 0.6 and these are simulated for abrupt change of load resistance from 40 Ω to 30Ω. These figures represent that all variables ( $i_{L1}$, $i_{L2}$, $|v_C|$ and $v_O$ ) of quantum Cuk PRC are good coincided with those of equivalent variables ( $i_{LB1}$, $i_{LB2}$, $|v_{CB}|$ and $v_{OB}$ ) of the conventional Cuk converters.

From these simulation comparisons, we know that the quantum Cuk PRC can be effectively modeled to conventional Cuk converter.

## VIII. CONCLUSIONS

QPRC operating on zero voltage switching conditions have been modeled as conventional Cuk, buck and boost converter which having an additional filter. Modeling have been verified by analytical methods and simulation results. From these modeling, it is shown that that parallel resonant circuit of the resonant converter is modeled as equivalent capacitance of the conventional converter. Dc and ac transfer functions of the QPRC have been derived by this analytical results and these are analogous to those of the conventional PWM converter except quantized characteristics due to quantized duty ratio. Therefore, the output voltage of the QPRC's can be controlled by proper feedback algorithm as those of conventional equivalent converters.

## REFERENCES


[1] G. B. Joung, C. T. Rim and G. H. Cho, "Modeling of quantum series resonant converters-controlled by integral cycle mode, "IEEE IAS Rec., PP. 821-826, 1988.

[2] G. B. Joung, C. T. Rim, and G. H. Cho, "An integral cycle mode control of series resonant converter, "IEEE PESC Rec., PP.575-582, 1988.

[3] K. H. Liu, R. Oruganti and F. C. Y. Lee, "Quasi-resonant converter topologies and characteristics, "IEEE Tran. on Power Electronics, vol PE-I, PP.62-71, Jan. 1987.

[4] D. M. Divan and G. L. Skibinski, "Zero switching loss inverter for high power applications, "IEEE-IAS Annual conference records, 1987, PP. 626-339.

[5] Ira J. Pitel, "Phase-modulated resonant power conversion techniques for high frequency link inverters, "IEEE Trans. Ind. Appl. vol. IA-22, No.6,PP. 1044-1051, Nov. 1986.

[6] Robert L. steigerwald, "High frequency resonant raansistor dc-dc converters, "IEEE Trans. Ind. Electronics. vol. IE-31, No.2, PP. 255-262, Aug. 1984

[7] R. J. King and T. A. sturat, "a large signal dysnamic simulation for the series resonant converter, "IEEE Tran. on Aerospace and Electronic systems. vol. AES-19. No.6,PP. 859-870, Nov. 1983

[8] M. H. Kheraluwala and D. M. Divan "Optimal discrete pulse modulation waveforms for resonant link inverter, "IEEE PESC Rec., PP. 567-574, 1988.

[9] W. M. Polivka, P. R. K. Chetty and R. D. Middlebrook, "State-space modeling of converters with parastics and storage time modulation, "in IEEE Power Electronics Specialists Conf.Rec., PP. 219-243, 1980.